Journal of Alloys and Compounds 617 (2014) 63–68

Contents lists available at ScienceDirect

Journal of Alloys and Compounds

journal homepage: www.elsevier.com/locate/jalcom

Synthesis, single crystal growth and properties of $Sr_5Pb_3ZnO_{12}$

M.J. Winiarski *, N.A. Szreder, R.J. Barczyński, T. Klimczuk *

Faculty of Applied Physics and Mathematics, Gdańsk University of Technology, ul. Narutowicza 11/12, 80-233 Gdańsk, Poland

ARTICLE INFO

Article history:
Received 6 May 2014
Received in revised form 15 July 2014
Accepted 21 July 2014
Available online 1 August 2014

Keywords:
Oxide materials
Solid state reactions
Crystal growth

ABSTRACT

The novel $Sr_5Pb_3ZnO_{12}$ oxide was synthesized by the solid-state reaction method. The crystal structure was studied by means of the powder X-ray diffraction Rietveld method and was found to be similar to 3 other previously known $Sr_5Pb_3MO_{12}$ compounds (M = Co, Ni, Cu). Crystals of several hundred microns in size of the new phase were grown in molten sodium chloride and imaged using confocal optical and scanning electron microscopy. Electrical properties were studied using the impedance spectroscopy technique. It was found that $Sr_5Pb_3ZnO_{12}$ is a dielectric material with rather high relative permittivity ($\varepsilon_r = 22$ at 300 K) and with activation energy of the dielectric relaxation process $E_A = 0.80(4)$ eV. The heat capacity studies reveal the Debye temperature $\Theta_D = 324(1)$ K.

1. Introduction

Oxide compounds that contain chains of transition metals are expected to reveal interesting electronic and magnetic properties [1]. Indeed one-dimensional Heisenberg antiferromagnetism was observed in $Ca_4Cu_5O_{10}$ [2], Peierls instability was found in $CuGeO_3$ [3] and spinon–holon separation in $SrCuO_2$ [4]. In the quasi-one-dimensional $BaVS_3$ sulfide compound, a metal-semiconductor transition and Luttinger behavior were reported [5].

One of the oxide systems with infinite chains of metals is $Sr_5Pb_3MO_{12}$ (M = Co, Ni, Cu). The first discovered $Sr_5Pb_3MO_{12}$ (531-M) compound was $Sr_5Pb_3CuO_{12+\delta}$ found as an impurity phase in the high-temperature superconductor BSCCO [6]. It has been synthesized by Babu and Greaves [7] and magnetic properties were studied by Yamaura et al. [8]. To date, two more 531-M compound were synthesized with M = Co, Ni, all having similar structure to 531-Cu [9,10]. Both 531-Cu and 531-Co are known to be dielectrics but no extensive studies of electrical properties were conducted. In $Sr_5Pb_{3-x}Bi_xMO_{12}$, Bi substitution for Pb does not significantly change the electrical conductivity but does change the one-dimensional antiferromagnetic properties [8].

In this study, polycrystalline samples of a novel 531-Zn compound were synthesized by solid-state reaction and electrically characterized. The structure of 531-Zn was studied using powder X-ray diffraction via the Rietveld refinement method.

2. Materials and methods

The polycrystalline $Sr_5Pb_3ZnO_{12}$ (531-Zn) sample was prepared by high-temperature solid state reaction. The precursor compounds: $SrCO_3$ (99.9%, Chempur), Pb_3O_4 (99%, Aldrich) and ZnO (99.9%, Aldrich) were weighted in stoichiometric amounts (assuming 5:3:1 Sr:Pb:Zn ratio), well ground and mixed using agate mortar and pestle and pressed into pellets, approx. 2 cm diameter, using a hydraulic press (pressure applied did not exceed 50 MPa) to obtain about 0.8 g of the 531-Zn compound. Pellets were placed in dense alumina crucible and annealed in a furnace at 750 °C for 36 h in air. The first step of the synthesis was intended to decompose the strontium carbonate without completing the solid-state reaction. The X-ray diffraction pattern measured on the powdered samples showed the presence of 531-Zn as well as $SrPbO_3$ phase [11,12] (about 30%). Pellets were then reground, repressed into smaller pellets (approx. 0.5 cm diameter, pressures applied to the sample did not exceed 300 MPa), placed in the same crucible used before and annealed in a furnace at 800 °C for 36 h in air. After this step, pellets were ground and preliminary X-ray diffraction measurement revealed that the sample was nearly single-phase, with minor quantities of $SrPbO_3$ impurity possibly present. The powder was then repressed into pellets and annealed at 850 °C for 36 h in air, and the product was found to be single phase 531-Zn. The same methodology was then successfully employed to synthesize polycrystalline pellets of 531-Cu and 531-Co for impedance spectroscopy measurements. CuO (99.5%, Reachim) and Co_2O_3 (99%, POCH) precursor materials were used, respectively. The other reactants used were the same as for 531-Zn.

To determine details of the crystal structure of the synthesized 531-Zn phase, a specimen was studied by powder X-ray diffraction in Bruker D8 FOCUS diffractometer with a Cu Kα radiation source. The diffraction pattern was analyzed by the Rietveld profile refinement method [13] using the FullProf 5.3 program [14]. The background was modeled using linear interpolation between 74 points with refinable intensity values.

To measure the oxygen content of the material, iodometric titration was conducted on a sample prepared as described previously, divided into 7 portions of approx. 0.2 g each [15,16]. Samples were dissolved in 100 ml of 0.33 M hydrochloric acid with approx. 7 g of potassium iodide and then titrated with 0.1 M sodium thiosulphate using starch as indicator (starch was added to the solution close to the endpoint of titration to avoid precipitation of iodine-starch complex [17]).

Iodine liberation reaction proceeds as follows:

* Corresponding authors.
E-mail addresses: mwiniarski@mif.pg.gda.pl (M.J. Winiarski), tomek@mif.pg.gda.pl (T. Klimczuk).

http://dx.doi.org/10.1016/j.jallcom.2014.07.156
0925-8388/

$$Pb^{4+} + 2I^- \rightarrow Pb^{2+} + I_2 \quad (1)$$

$$Pb^{2+} + 2I^- \rightarrow PbI_2 \downarrow \quad (2)$$

The second step of reaction resulted in formation of yellow precipitate of a similar appearance to 531-Zn powder. To determine if dissolution of 531-Zn was complete, XRD measurements were done on the filtered residue, which showed that the precipitate did not consist of 531-Zn, with only lead(II) iodide (PbI_2) present.

The crystal growth mineralization method was adapted from the study on 531-Ni [10]. Approximately 0.2 g of 531-Zn polycrystalline powder obtained after the second annealing (800 °C) was ground and mixed together with approx. 2 g of sodium chloride employed as a mineralizer. The powder was put in an alumina crucible covered with a lid within another crucible turned upside-down. The crucible was placed in an alumina boat and put into a chamber furnace. The temperature program used was: (1) ramping to 950 °C at 180 C/h, (2) holding 950 °C for 3 h to homogenize the sample, and (3) slow cooling at 6 °C/h to 790 °C (below the NaCl melting point) and switching the furnace off. The contents of the crucible were then rinsed with distilled water, filtered and dried. Then it was examined using Scanning Electron Microscope (FEI Quanta) working in low-vacuum environmental mode (chamber pressure 130 Pa, water vapor) and using Olympus LEXT OLS4000 confocal scanning laser microscope (CSLM). The red-brown powder obtained forms small needle-like crystals that have a rod-type shape with clearly visible hexagonal faces (Fig. 1). The largest of the single-crystals were approximately 700 μm long and 70 μm wide.

EDS spectroscopy was conducted in low-vacuum conditions due to heavy specimen charging, with the electron energy set to 20 keV. EDS spectra were collected on 19 points for 9 distinct single crystals with an acquisition time of 100 s. Further analysis was performed by using EDAX TEAM™ software by means of a standardless analysis with the *eZAF* quantization method. Fig. 1(e) shows a sample EDS spectra collected for a single crystal.

Although the crystal growth was successful, the crystals were too small to measure the physical properties. The crystal growth process parameters (especially the cooling rate) should be optimized to obtain crystals of larger dimensions, suitable for physical property measurements.

For the dielectric studies, a small cylindrical pellet (diameter 4.78 mm, height 0.66 mm) of 531-Zn was polished and gold contacts were sputtered on both its basal surfaces. A mask with a hole with slightly smaller diameter was used to protect the lateral surface of the sample. A sample prepared this way was used for impedance spectroscopy measurements conducted with a Novocontrol Concept 40 broadband dielectric spectrometer in a temperature range from −120 to +150 °C (step 30 °C) and frequency range 10 mHz–10 MHz. The applied voltage (RMS) used was set to 1.0 V. Nyquist plots resulting from the measurements were fitted with equivalent circuit using Scribner ZView 2 program. The parameters of the circuit elements were refined using the least squares method.

Heat capacity measurements were performed in a Quantum Design Physical Property Measurement System using the standard relaxation calorimetry method. A small piece (about 6 mg) of sample was measured in the temperature range of 1.9–300 K.

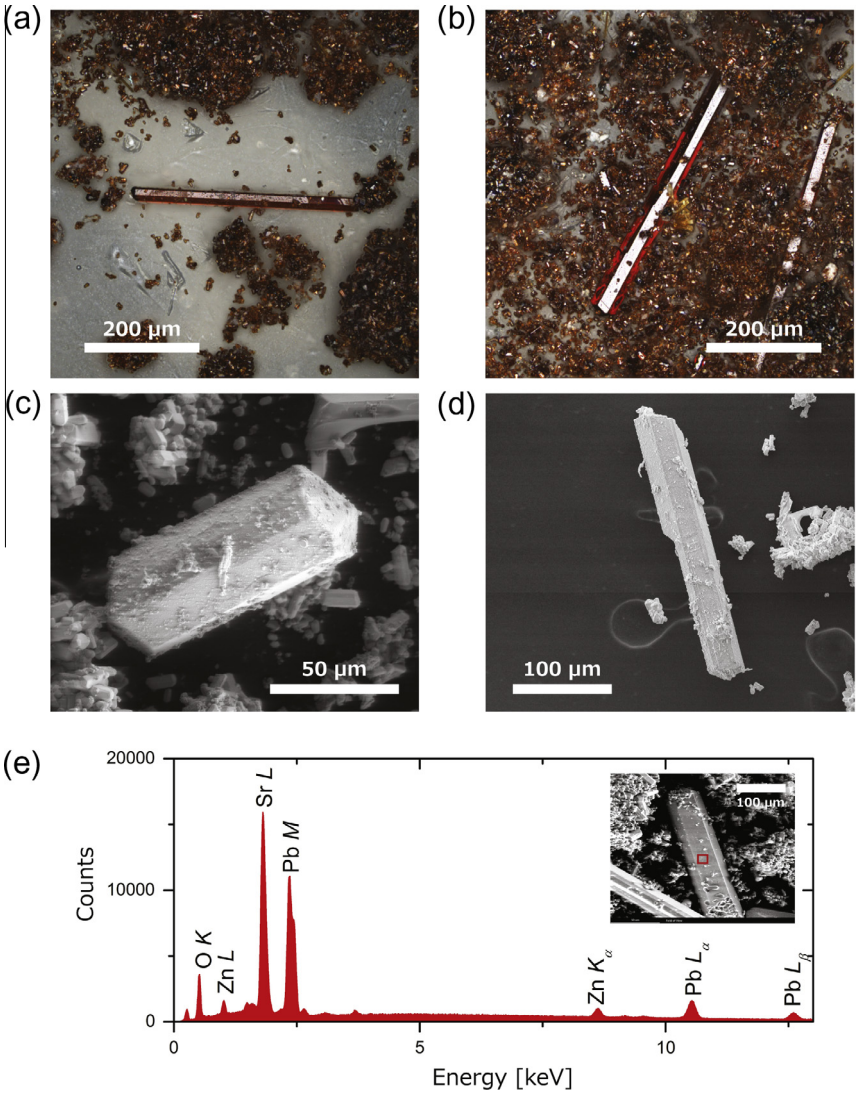

Fig. 1. CSLM (a, b) and SEM (c, d) micrographs of 531-Zn single crystals with sample EDS spectrum for the single crystal (e). The inset of (e) shows the single crystal from which the spectrum was collected with the scanned area indicated by a red rectangle. (For interpretation of the references to color in this figure legend, the reader is referred to the web version of this article.)

3. Results and discussion

The observed X-ray spectra for $Sr_5Pb_3ZnO_{12}$, the calculated powder-diffraction pattern, the difference between the calculated model and experimental data, and the positions of expected Bragg peaks are presented in Fig. 2. The model used for refinement was derived from the structure of 531-Co [9]. Cell and atomic parameters are shown in Table 1.

The crystal structure of the new compound was found to be similar to other known 531-M compounds. In particular, the transition metal ion (Zn^{2+}) is situated in a trigonal prismatic site, and ZnO_6 and PbO_6 polyhedra form infinite chains along the *c*-axis, surrounded by Sr^{2+} ions as is shown in Fig. 3(c) and (d). The Zn position is half-occupied and the Zn-O polyhedra are significantly distorted, as it is visible in Fig. 3(d).

The major difference between the observed and calculated intensity is for the (300) and (111) reflections, in the 2Θ angle range 30.5° and 30.8°. This difference is possibly caused by insufficient modeling of ZnO_6–PbO_6 chains. The large value of thermal parameter for Zn suggests that the local environment of Zn atoms is more complex than it is deduced from our refinement. Neutron powder diffraction studies of 531-Cu ran into the same issue [7], with the authors pointing out possible cation disorder and deviation from the $Sr_5Pb_3MO_{12}$ stoichiometry. Our EDS studies performed on single crystals, confirm the 5:3:1 (Sr:Pb:Zn) cation ratio. Results of the iodometric titration yield the concentration of Pb^{4+} ions $x_{Pb^{4+}} = 3.1(2)$ ions per formula unit. This suggests that Pb in 531-Zn is present in +4 oxidation state, and because Zn can only exist in +2 form, the oxygen stoichiometry is 12 atoms per formula unit. Therefore in 531-Zn we do not expect additional oxygen atoms that partially occupy 6*i* sites as it was reported for 531-Cu [8] and 531-Co [9] compounds. The substoichiometric concentration of the oxygen in 531-Zn is unlikely due to the fact that synthesis was conducted in air at relatively low temperature. It is in agreement with the titration results that does not suggest the presence of Pb^{2+} ions.

The physical properties of 531-Zn were first studied by the impedance spectroscopy technique; the results are shown in Fig. 4. The Nyquist plot for the 531-Zn sample consists of one

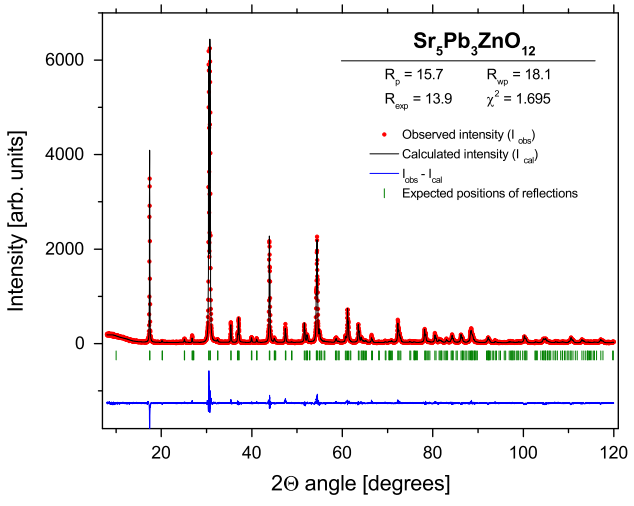

Fig. 2. Fit (solid black line) of the refined structural model (Rietveld method) to the room-temperature X-ray powder diffraction data (red circles) for 531-Zn. Upper part: circles – observed data, solid line – calculated intensities. The lower part (blue line) shows the differences between the observed and calculated pattern. The green bars correspond to 531-Zn. (For interpretation of the references to color in this figure legend, the reader is referred to the web version of this article.)

Table 1
Crystallographic data for 531-Zn obtained using Rietveld refinement. Figures of merit: profile residual $R_p = 10.3\%$, weighted profile residual $R_{wp} = 13.7\%$, expected profile residual $R_{exp} = 10.49\%$, goodness of fit $\chi^2 = 1.70$.

Basic crystallographic data					
Compound formula	$Sr_5Pb_3ZnO_{12}$				
Molar mass (g/mol)	1317.0828				
Space group	$P\bar{6}2m$, no. 189				
a (Å)	10.1277(1)				
c (Å)	3.53488(4)				
Cell volume (Å^3)	313.997(6)				
Calculated density (g/cm^3)	6.965				
Atom	*x*	*y*	*z*	*B* (Å^2)	SOF
Atomic parameters					
Sr(1)	$\frac{1}{3}$	$\frac{2}{3}$	$\frac{1}{2}$	1.71(18)	1
Sr(2)	0.6965(4)	0	$\frac{1}{2}$	0.83(11)	1
Pb	0.3377(2)	0	0	1.09(2)	1
Zn	0	0	0.2751(51)	6.69(55)	0.5
O(1)	0.1779	0	$\frac{1}{2}$	–	1
O(2)	0.4617	0	$\frac{1}{2}$	–	1
O(3)	0.2380	0.4428	0	–	1

semicircle and therefore a simple resistor-CPE model was chosen to fit the experimental data, as shown in Fig. 4(b). The DC conductivity obtained from the fit was $\sigma_{DC} = 2.43(6) \cdot 10^{-14}\ \Omega^{-1}\ cm^{-1}$ at 300 K. For the two other 531-M compounds, 531-Cu and 531-Co, in the Nyquist plot two semicircles are visible (Fig. 4(d)) which suggest the presence of two relaxation mechanisms. The existence of two relaxation mechanisms as well as significantly lower resistivity than in the case of 531-Zn has been attributed to a mixed valency state of Cu and Co [8,9]. The conduction mechanism in 531-Cu and 531-Co is possibly an electron transfer between Cu^{2+} and Cu^{3+} ions in 531-Cu (Co^{2+} and Co^{3+} in 531-Co).

DC resistivity values derived from fitted parameter were plotted against the temperature and activation energy of the conduction process was calculated using Arrhenius relation:

$$\rho(T) = \rho_0 \exp\left(\frac{E_a}{k_B T}\right) \tag{3}$$

where: E_a – activation energy, k_B – Boltzmann constant. Fig. 5(a) and (b) shows the plot of $\ln(\rho) = f(T^{-1})$ and $\rho = f(T)$, respectively. Activation energy of the relaxation process has a value of $E_A = 0.80(4)$ eV. Relative dielectric permittivity, ε_r, is almost frequency independent in a wide range of frequencies, and has a value of about 22 at 300 K.

The overall temperature dependence of the specific heat C_p is shown on Fig. 6. The heat capacity of the sample at room temperature (~ 450 J mol^{-1} K^{-1}) is close, but slightly lower than the value expected from the Dulong–Petit Law ($3nR \approx 524$ J mol^{-1} K^{-1}), where *n* is number of atoms per formula unit and *R* is the gas constant).

Fig. 7 shows specific heat divided by temperature as a function of temperature squared $\left(\frac{C_p}{T} = f(T^2)\right)$ in the low-temperature range measured under zero magnetic field. Data points were fit in the temperature range of 2.3–6.5 K using the formula $\frac{C_p}{T} = \gamma + \beta T^2$. The value of Sommerfeld coefficient obtained from the fit is $\gamma = 0.14(19)$ mJ mol^{-1} K^{-2}, which is close to zero, as expected for a dielectric material. The phonon specific-heat coefficient $\beta = 1.194(9)$ J mol^{-1} K^{-4}. In a simple Debye model, at low temperature the β coefficient is related to the Debye temperature Θ_D through the relation given in Eq. (4):

$$\Theta_D = \sqrt[3]{\frac{12\pi^4 nR}{5\beta}} \tag{4}$$

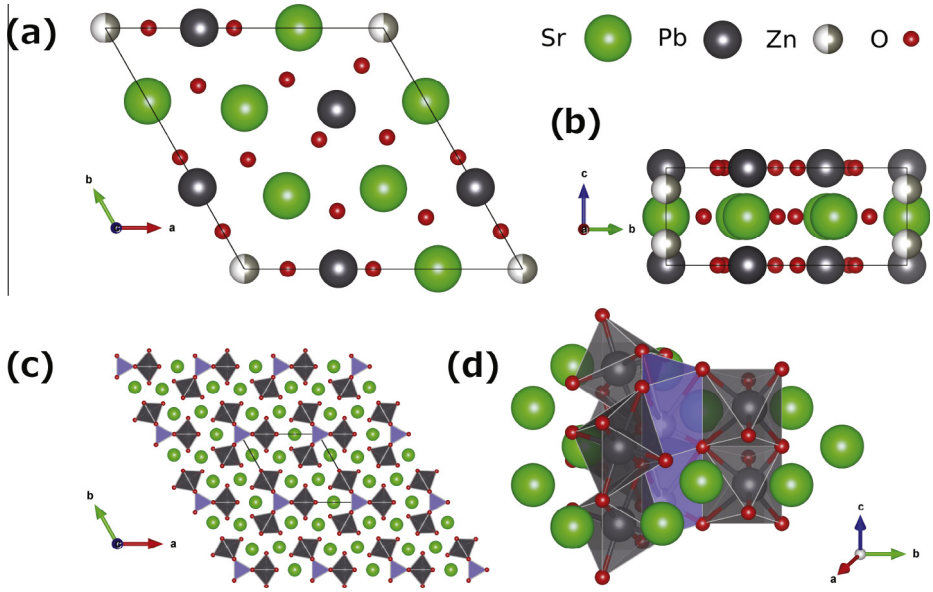

Fig. 3. Visualisation of the crystal structure rendered with VESTA software [18]: (a) unit cell viewed along the *c* axis, (b) unit cell viewed along the *a* axis, (c) view along the *c* axis revealing the triple-symmetry of ZnO_6–PbO_6 chains surrounded by Sr^{2+}, and (d) a close-up of one element of the chain. Zn atoms are half-colored to emphasize that this position is half-occupied.

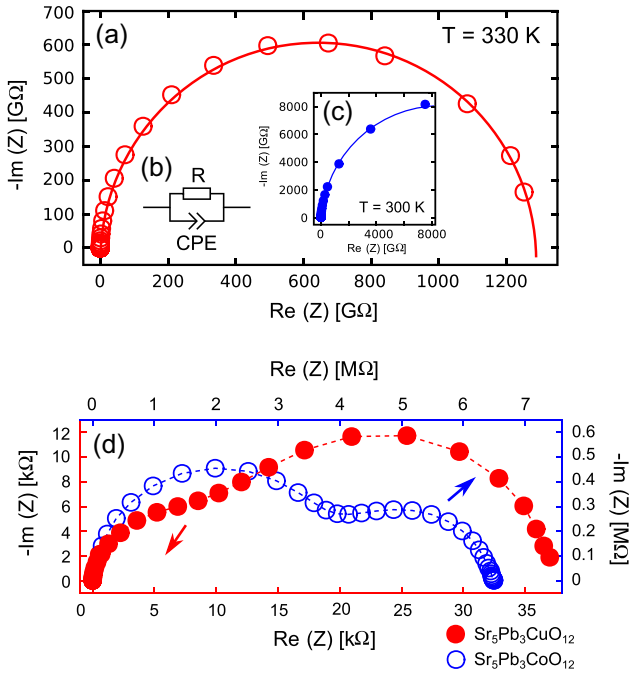

Fig. 4. Nyquist plot for 531-Zn at 330 K showing one relaxation mechanism (a), solid line is a guide for eyes. (b) The equivalent circuit used for fitting, (c) Nyquist plot for 531-Zn at 300 K, (d) Nyquist plots for samples of 531-Cu (red filled circles) and 531-Cu (blue circles) synthesized and measured with the same methodology as 531-Zn. (For interpretation of the references to color in this figure legend, the reader is referred to the web version of this article.)

The Debye temperature calculated from this relation $\Theta_D = 324(1)$ K. The specific heat calculated from the Debye model with this value of Θ_D is not large enough to reach the experimental values measured at the higher temperatures, therefore the data in the whole temperature range was fit by using the formula given in Eq. (5), which includes the contribution of higher-energy optical modes:

$$C_p(T) = \gamma T + k \cdot C_D(T) + (1-k) \cdot C_E(T) \quad (5)$$

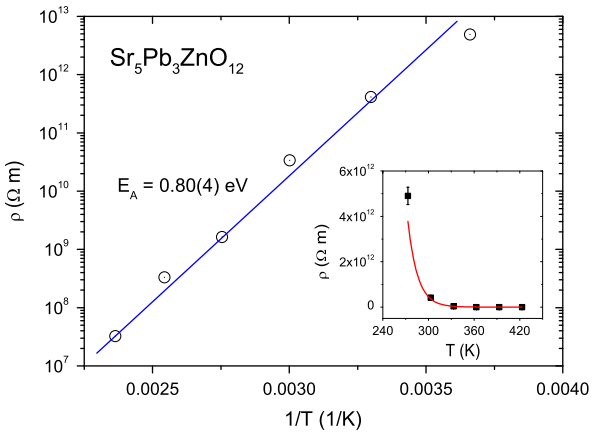

Fig. 5. Natural logarithm of resistivity vs. inverse temperature (a) and resistivity vs. temperature (b) plots. Black points – values obtained from Nyquist plots, solid lines – fit to the data. (For interpretation of the references to color in this figure legend, the reader is referred to the web version of this article.)

where C_D and C_E are specific heat functions derived from the Debye and Einstein models, respectively, the k parameter corresponds to the weight of the phonon contributions to the specific heat from both models, and γ is the Sommerfeld coefficient. Such an approach is commonly used in case of intermetallic compounds and was employed for the whole temperature range fitting of specific heat data for $Mg_{10}Ir_{19}B_{16}$ [19] and UCr_2Al_{20} [20]. As shown by the low temperature fit, the electronic heat capacity, γT, is negligible. The temperature dependence of the specific heat for Debye and Einstein models is given in Eqs. (6) and (7), respectively:

$$C_D(T) = 9nR\left(\frac{T}{\Theta_D}\right)^3 \int_0^{x_D} \frac{x^4 \exp(x)}{(\exp(x)-1)^2} dx \quad (6)$$

$$C_E(T) = 3nR\left(\frac{\Theta_E}{T}\right)^2 \exp\left(\frac{\Theta_E}{T}\right)\left(\exp\left(\frac{\Theta_E}{T}-1\right)\right)^{-2} \quad (7)$$

where $x = \frac{h\nu}{k_B T}$ and $x_D = \frac{\Theta_D}{T}$, Θ_D and Θ_E being Debye and Einstein temperatures, respectively. The fit, plotted as a solid red line in Fig. 6,

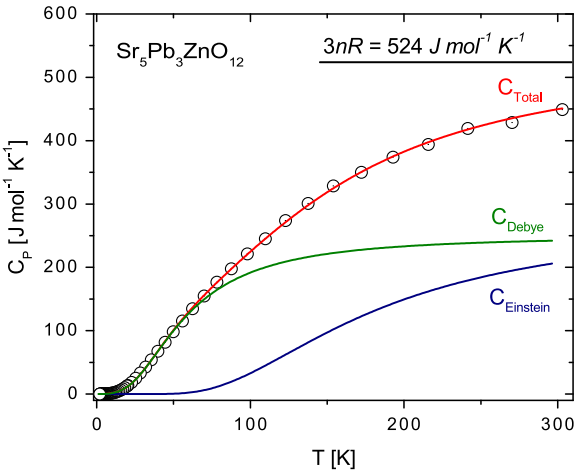

Fig. 6. Specific heat vs. temperature for 531-Zn. Points – measured specific heat, solid red line – fit to the measured data (Eq. (5)), green line – the Debye part of the total specific heat, blue line – the Einstein part of the total specific heat. Black solid line indicates the value calculated from the Dulong Petit Law. (For interpretation of the references to color in this figure legend, the reader is referred to the web version of this article.)

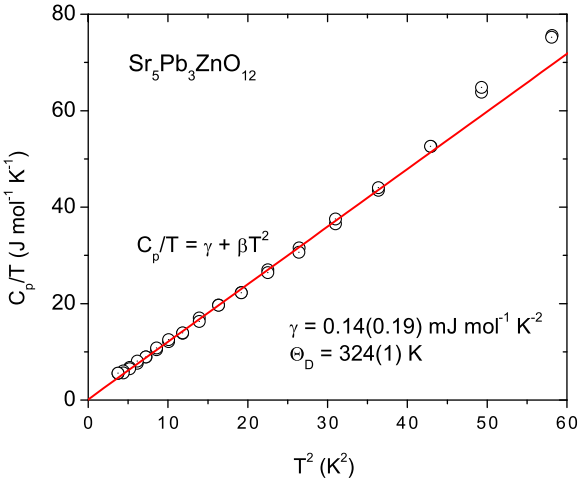

Fig. 7. Specific heat divided by temperature as a function of the temperature squared for 531-Zn. Points – values measured in PPMS, red solid line – linear fit to the low temperature part of $\frac{C_p}{T} = f(T^2)$. (For interpretation of the references to color in this figure legend, the reader is referred to the web version of this article.)

gives $k = 48\%$ of the weight to the Debye contribution with $\Theta_D = 237(2)$ K and $(1-k) = 52\%$ to Einstein term with $\Theta_E = 556(4)$ K.

4. Conclusions

A novel solid-state compound, $Sr_5Pb_3ZnO_{12}$ (531-Zn), was synthesized and characterized. The structure of the new compound closely resembles the structures of the other 531-M oxides. In contrast to the 531-M (M = Co, Cu, Ni) compounds, the oxygen stoichiometry for 531-Zn is 12 per formula unit and no additional oxygen atoms partially occupying the 6*i* sites are expected. A single-crystal growth experiment showed that needle-like crystals can be grown using simple mineralization method with NaCl as the mineralizer. Process parameters (especially cooling rate) should be optimized to grow crystals suitable for measuring physical properties.

531-Zn was found to be a dielectric with rather high relative permittivity ($\varepsilon_r = 22$ at 300 K) and with one relaxation mechanism visible in the examined range of temperature and frequency. This is in contrast with results for 531-Cu and 531-Co, where two mechanisms are observed. The conductivity activation energy for 531-Zn was estimated by using the Arrhenius fit and its value is $E_A = 0.80(4)$ eV. As expected for insulators, the Sommerfeld coefficient (γ) estimated from the heat capacity measurement, is equal to zero (within the uncertainty). The low temperature fit gives the Debye temperature $\Theta_D = 324(1)$ K for 531-Zn.

Future studies would involve doping of 531-Zn to determine whether an insulator-to-metal transition can be induced. One unconfirmed report of a metal–insulator transition accompanied by a strong structural modulation and possible superconductivity in a heavily La-doped 531-Cu compound has been published [21] but no further studies have been conducted on this apparent superconductor to the authors knowledge.

Acknowledgements

The project was partially supported by the Polish National Science Centre (Decision no. DEC-2012/07/E/ST3/00584).

The authors acknowledge helpful discussions with Robert J. Cava (Princeton University).

References

[1] T.N. Nguyen, P.A. Lee, H.-C. z. Loye, Design of a random quantum spin chain paramagnet: $Sr_3CuPt_{0.5}Ir_{0.5}O_6$, Science 271 (5248) (1996) 489–491, http://dx.doi.org/10.1126/science.271.5248.489.

[2] M. Imada, A. Fujimori, Y. Tokura, Metal–insulator transitions, Rev. Mod. Phys. 70 (4) (1998) 1039–1263, http://dx.doi.org/10.1103/RevModPhys.70.1039.

[3] M. Hase, I. Terasaki, K. Uchinokura, Observation of the spin-Peierls transition in linear Cu^{2+} (spin-1/2) chains in an inorganic compound $CuGeO_3$, Phys. Rev. Lett. 70 (23) (1993) 3651–3654, http://dx.doi.org/10.1103/PhysRevLett.70.3651.

[4] C. Kim, A.Y. Matsuura, Z.-X. Shen, N. Motoyama, H. Eisaki, S. Uchida, T. Tohyama, S. Maekawa, Observation of spin-charge separation in one-dimensional $SrCuO_2$, Phys. Rev. Lett. 77 (19) (1996) 4054–4057, http://dx.doi.org/10.1103/PhysRevLett.77.4054.

[5] M. Nakamura, A. Sekiyama, H. Namatame, A. Fujimori, H. Yoshihara, T. Ohtani, A. Misu, M. Takano, Metal-semiconductor transition and Luttinger-liquid behavior in quasi-one-dimensional $BaVS_3$ studied by photoemission spectroscopy, Phys. Rev. B 49 (23) (1994) 16191–16201, http://dx.doi.org/10.1103/PhysRevB.49.16191.

[6] J. Kim, X. Tang, A. Manthiram, J. Swinnea, H. Steinfink, A new phase in the SrPbCu oxide system: the crystal structure of $Sr_{5-x}Pb_{3+x}Cu_yO_{12-\delta}$, J. Solid State Chem. 85 (1) (1990) 44–50, http://dx.doi.org/10.1016/S0022-4596(05)80058-1.

[7] T. Babu, C. Greaves, A neutron powder diffraction study of the phase $Sr_5Pb_3CuO_{12}$, J. Solid State Chem. 95 (2) (1991) 417–423, http://dx.doi.org/10.1016/0022-4596(91)90123-Y.

[8] K. Yamaura, Q. Huang, E. Takayama-Muromachi, Crystal structure and magnetism of the linear-chain copper oxides $Sr_5Pb_{3-x}Bi_xCuO_{12}$, Phys. Rev. B 64 (18) (2001) 184428, http://dx.doi.org/10.1103/PhysRevB.64.184428.

[9] K. Yamaura, Q. Huang, E. Takayama-Muromachi, Synthesis, crystal structure, and magnetic properties of the linear-chain cobalt oxide $Sr_5Pb_3CoO_{12}$, J. Solid State Chem. 164 (1) (2002) 12–18, http://dx.doi.org/10.1006/jssc.2001.9420.

[10] T.J. Prior, P.D. Battle, Pentastrontium trilead nickel dodecaoxide, $Sr_5Pb_3NiO_{12}$, J. Chem. Crystallogr. 34 (4) (2004) 255–258, http://dx.doi.org/10.1023/B:JOCC.0000022424.94105.94.

[11] H.L. Keller, K.H. Meier, H. Mueller-Buschbaum, Zur Kristallstruktur von $SrPbO_3$, Z. Naturforsch., Teil B 30 (1975) 277–278.

[12] S. Grazulis, D. Chateigner, R.T. Downs, A.F.T. Yokochi, M. Quiros, L. Lutterotti, E. Manakova, J. Butkus, P. Moeck, A. Le Bail, Crystallography open database – an open-access collection of crystal structures, J. Appl. Crystallogr. 42 (Pt 4) (2009) 726–729, http://dx.doi.org/10.1107/S0021889809016690.

[13] H.M. Rietveld, A profile refinement method for nuclear and magnetic structures, J. Appl. Crystallogr. 2 (2) (1969) 65–71.

[14] J. Carvajal, FULLPROF: a program for Rietveld refinement and pattern matching analysis, in: Abstracts of the Satellite Meeting on Powder Diffraction of the XV Congress of the IUCr, Tolouse, France, 1990, p. 127.

[15] D.C. Harris, M.E. Hills, T.A. Hewston, Preparation, iodometric analysis, and classroom demonstration of superconductivity in $YBa_2Cu_3O_{8-x}$, J. Chem. Educ. 64 (10) (1987) 847, http://dx.doi.org/10.1021/ed064p847.

[16] S. Scheurell, E. Kemnitz, G.N. Maso, S.Y. Kasin, S.W. Naumov, Y.N. Badun, Determination of the complete stoichiometry of Bi–Pb–Sr–Ca–Cu–O-superconductors, Fresenius' J. Anal. Chem. 340 (6) (1991) 353–356, http://dx.doi.org/10.1007/BF00321581.

[17] M. Karppinen, M. Matvejeff, K. Salomaki, H. Yamauchi, Oxygen content analysis of functional perovskite-derived cobalt oxides, J. Mater. Chem. 12 (6) (2002) 1761–1764.
[18] K. Momma, F. Izumi, VESTA 3 for three-dimensional visualization of crystal, volumetric and morphology data, J. Appl. Crystallogr. 44 (6) (2011) 1272–1276.
[19] T. Klimczuk, Q. Xu, E. Morosan, J.D. Thompson, H.W. Zandbergen, R.J. Cava, Superconductivity in noncentrosymmetric $Mg_{10}Ir_{19}B_{16}$, Phys. Rev. B 74 (22) (2006) 220502.
[20] P. Swatek, D. Kaczorowski, Magnetic and electrical properties of UCr_2Al_{20} single crystals, J. Solid State Chem. 191 (2012) 191–194.
[21] G.C. Che, J.Q. Li, H. Jiang, C. Dong, G.D. Liu, S.L. Jia, Z.X. Zhao, Metal-insulator transition and possible superconductivity in $Pb_{2.2}Cu_{0.8}Sr_{3.1}La_{1.5}Cu_{1.5}O_y$ with hexagonal structure, Mater. Res. Innovations 3 (4) (2000) 212–217, http://dx.doi.org/10.1007/s100190050005.